DNS OF CHANNEL FLOW WITH CONJUGATE HEAT TRANSFER - BUDGETS OF TURBULENT HEAT FLUXES AND TEMPERATURE VARIANCE

C. Flageul[1], S. Benhamadouche[1], E. Lamballais[2] and D. Laurence[1,3]

[1]EDF R&D, Fluid Mechanics, Energy and Environment Dept. 6 Quai Wattier, 78401 Chatou, France

[2] Institute PPRIME, Department of Fluid Flow, Heat Transfer and Combustion, Université de Poitiers, CNRS, ENSMA, Téléport 2 - Bd. Marie et Pierre Curie B.P. 30179, 86962 Futuroscope Chasseneuil Cedex, France

[3]School of Mechanical, Aerospace and Civil Engineering, The University of Manchester, Sackville Street, Manchester M60 1QD, UK

cedric.flageul@edf.fr

1 Introduction

More than 40 years ago, Direct Numerical Simulation started with the pioneering work of Orszag (1971). This powerful workbench to study turbulence tempts more and more people as the computational power available increases. Only few DNS dealt with conjugate heat transfer issues. To the authors' knowledge, Tiselj et al. (2001a) were among the first to investigate this more realistic situation in a channel flow using pseudo-spectral methods. Kang et al. (2009) performed Quasi-DNS with conjugate heat transfer of a heated cylinder in a channel using immersed boundaries and a fully implicit LES solver based on unstructured collocated mesh using finite volume approach.

Conjugate heat transfer simulations are needed in industrial applications where fluctuating thermal stresses are a concern, in case of a severe emergency cooling or long ageing materials. High Reynolds RANS and LES simulations rely on wall-modeling as the viscous sub-layer is not resolved. DNS is a valuable tool for understanding the flow physics of such complex phenomena and to provide fine data in order to improve RANS and LES approaches.

The present work provides budgets of turbulent heat fluxes and temperature variance for a channel flow with different thermal boundary conditions: an imposed temperature, an imposed heat flux and with conjugate heat transfer combined with an imposed heat flux at the outer wall.

2 Numerical approach

Present simulations are based on the open-source software Incompact3d developed at Université de Poitiers and Imperial College London (http://code.google.com/p/incompact3d/) by Laizet et al. (2009, 2011). Sixth-order compact finite difference schemes are used on a Cartesian grid. The pressure is computed on a staggered grid using a spectral approach while velocity's components and temperature are collocated.

The incompressible Navier-Stokes and energy equations of a fluid with constant properties (1) and (2) are solved using a projection method (eqs (3) and (4)). The convective term in the momentum equation is computed using the skew-symmetric form.

$$\partial_i u_i = 0 \quad \partial_t u_i + \partial_j (u_i u_j) = -\partial_i p + \frac{1}{\mathrm{Re}} \partial_{jj} u_i \quad (1)$$

$$\partial_t T + \partial_j (T u_j) = \frac{1}{\mathrm{Re}\,\mathrm{Pr}} \partial^2_{jj} T \quad (2)$$

$$\frac{u_i^* - u_i^n}{\Delta t} = \frac{\left(\partial_{yy} u_i^* + \partial_{yy} u_i^n\right)}{2\,\mathrm{Re}} + F_i\left(u^n, u^{n-1}, p^n\right) \quad (3)$$

$$\frac{u_i^{n+1} - u_i^*}{\Delta t} = -\partial_i \delta p^{n+1} \quad (4)$$

The convective and the wall-parallel viscous terms are integrated through a 2nd order Adams-Bashforth time advancing scheme and the wall-normal viscous term through a Crank-Nicolson one. The numerical approach is exactly the same for the fluid temperature. While performing conjugate heat transfer, the diffusion equation for the temperature in the solid is given by eq. (5):

$$\frac{T_s^{n+1} - T_s^n}{\Delta t} = \frac{1}{G\,\mathrm{Re}\,\mathrm{Pr}} \partial^2_{yy} T_s^{n+1} + F\left(T_s^n, T_s^{n-1}\right) \quad (5)$$

The thermal diffusivity ratio G is set to unity for the present computations. The solid domain is on top ($y \geq L_y$) and on the bottom ($y \leq 0$) of the fluid domain. The thermal solver for the solid domain uses *finite differences* for the wall-parallel diffusion and a *spectral* method for the wall-normal one. Time-advancement is similar to the flow except for the wall-normal diffusion that is fully implicit.

The thermal coupling between both solvers is performed as follow. First, the fluid temperature is

subjected to a Dirichlet boundary condition: $T^{n+1} = \left(T^n + T_s^n\right)/2$. Then, the solid temperature is subjected to a Neumann boundary condition: $\partial_n T_s^{n+1} = \beta \partial_n T^{n+1}$. The ratio of thermal conductivities β is set to unity for the present computations. Tthe coupling strategy is first order in time: the resulting temperature field is slightly discontinuous at the interface while the heat flux is continuous through the Neumann boundary condition.

The set of coefficients used in the fluid domain with compact finite difference schemes for the collocated derivatives ($\partial_c^1, \partial_c^2$), the staggered derivation (∂_s^1) and the staggered interpolation (I_s) are recalled table 1. Only approximated values are given here for ∂_c^2 (Lamballais et al. (2011) with $k_c''\Delta x^2 = 4\pi^2$).

	∂_c^1	∂_c^2	∂_s^1	I_s
α	1/3	0.478	9/62	3/10
a	14/9	0.421	63/62	3/2
b	1/9	1.70	17/62	1/10
c	0	-0.164	0	0

Table 1: Finite difference coefficients

In the solid domain, the finite difference scheme is the only 6th order non-compact centered scheme with a stencil of 7 points.

3 Configuration, Results

A channel flow with a Reynolds number (based on the bulk velocity and the channel half-height) of 2280 is simulated with a Prandtl number of 0.71. The reference simulations are from Kasagi et al. (1992) which uses a Dirichlet boundary condition for the temperature and from Tiselj et al. (2001a) which uses a Neumann boundary condition for the temperature. Table 2 gives a comparison for the main parameters between our simulation and Kasagi et al. (1992).

	Present	Ref
Domain	[12.8; 2; 4.26]	[5π; 2; 2π]
Grid	[256;193;256]	[128;97;128]
Re_τ	148.8	150
Δy^+	[0.49; 4.8]	[0.08; 4.9]
$[\Delta x^+, \Delta z^+]$	[7.4; 2.5]	[18.4; 7.36]
Δt^+	0.02	0.12
Duration	16000	2100

Table 2: Simulation parameters. Ref: Kasagi et al. (1992)

The flow rate is imposed with a source term in the momentum equation. The source term in the energy equation is similar to the one used by Kasagi et al. (1992) and balances the overall heat input at the walls. The simulation with a temperature imposed at the boundary is called isothermal. The one with a heat flux imposed is called isoflux. For the case with conjugate heat transfer, the solid domain size is [12.8; 1; 4.26], located on top and bottom of the fluid domain, as sketched figure 1. The external faces of the solid domain are subjected to a constant heat flux, equal to the one imposed in the isoflux case.

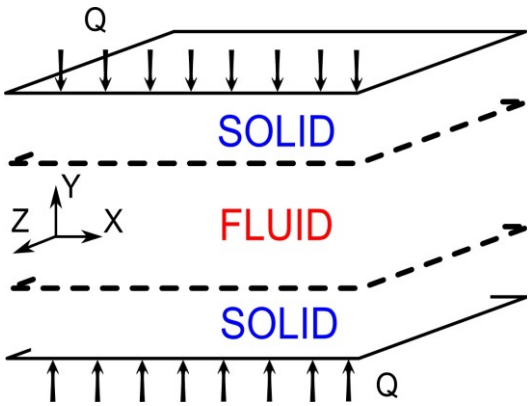

Figure 1: Sketch of the configuration.

As shown figures 2 and 3, the present compact finite-difference simulation compares well with the pseudo-spectral results of Kasagi et al. (1992), even for high order statistics such as the budgets of the turbulent heat fluxes.

In figure 4, turbulent heat fluxes and the temperature variance for the isoflux case are in perfect agreement with the results of Tiselj et al. (2001a).

Budgets for the isoflux case are available for a flume configuration (Tiselj et al. (2001b)) and for a concentric annular pipe flow (Chung et al. (2003)). However, to the authors' knowledge, no budgets are available in the literature when the heat flux is imposed or in case of conjugate heat transfer for the channel flow configuration. It is therefore interesting to compare the budgets for isoflux and conjugate simulations with their isothermal counterparts.

In figure 5, the molecular diffusion and the dissipation behave differently in the near-wall region. They have lower amplitude in the isoflux case compared with the isothermal one. The behavior is similar for the budgets of the temperature variance with lower amplitudes obtained in the isoflux case.

In figure 6, the situation is similar for conjugate heat transfer: the molecular diffusion and the dissipation rate have lower amplitude in the near-wall region when compared with the isothermal case. In fact, for most of the statistics, a 3-way comparison puts conjugate heat transfer in-between isothermal and isoflux results, as expected. The impact of the thermal boundary condition on some statistical quantities is important when $y^+ \leq 20$, especially for the dissipation and the molecular diffusion associated with the streamwise turbulent heat flux and the temperature variance, in agreement with the results in Kasagi et al. (1989).

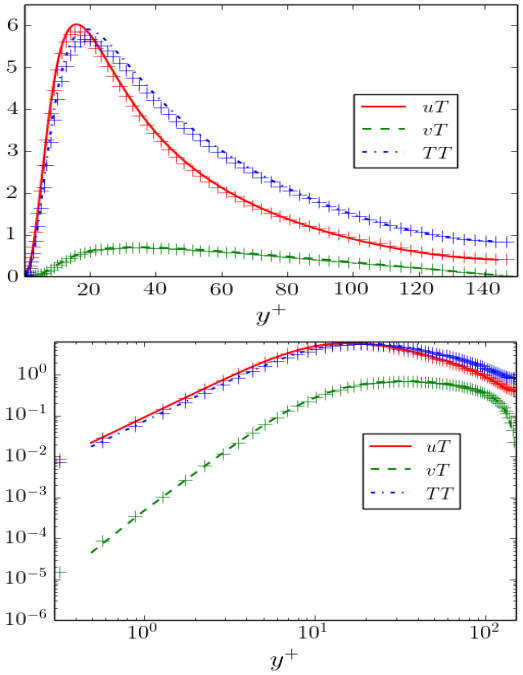

Figure 2: Isothermal b.c., turbulent heat fluxes and temperature variance. Line: present. Symbol: Kasagi et al. (1992).

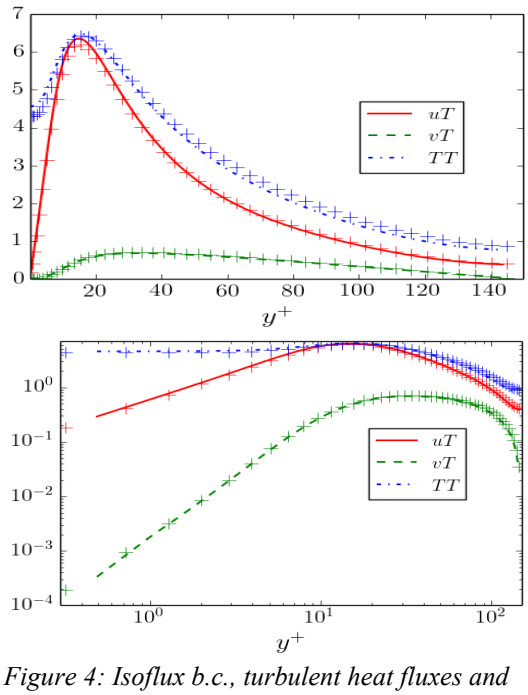

Figure 4: Isoflux b.c., turbulent heat fluxes and temperature variance. Line: present. Symbol: Tiselj et al. (2001a).

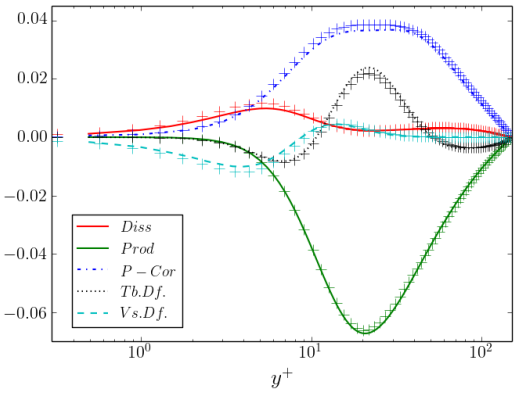

Figure 3: Isothermal b.c., budget of wall-normal turbulent heat flux. Line: present. Symbol: Kasagi et al. (1992).

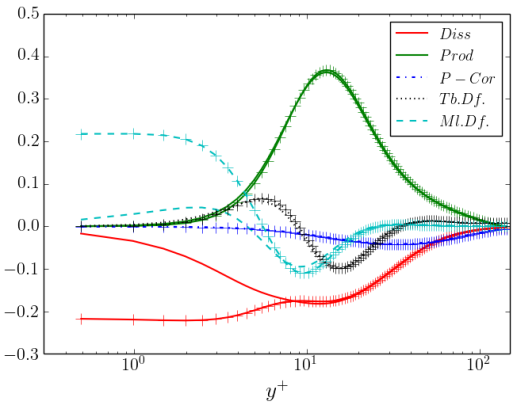

Figure 5: Budget of axial turbulent heat flux. Line: isoflux b.c. Line+Symbol: isothermal b.c.

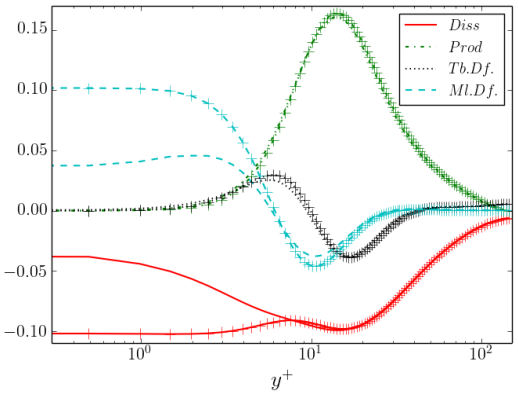

Figure 6: Budget of temperature variance. Line: conjugate. Line+Symbol: isothermal b.c.

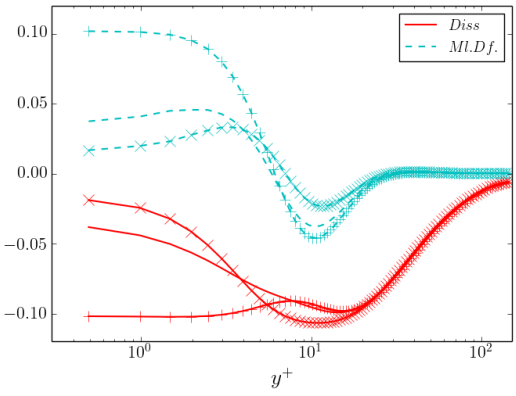

Figure 7: Molecular diffusion and dissipation of the temperature variance. Line: conjugate. Line+Symbol: isothermal b.c.(+) and isoflux b.c.(x)

4 Asymptotic analysis ($y \to 0$)

The near-wall instantaneous temperature and velocity fields can be approached using a Taylor expansion (eqn. (6)-(9)) where the coefficients depend on (x,z,t).

$$T(x,y,z,t) = a + by + cy^2 + \ldots \quad (6)$$

$$u_1 = b_1 y + c_1 y^2 + \ldots \quad (7)$$

$$u_2 = c_2 y^2 + \ldots \quad (8)$$

$$u_3 = b_3 y + c_3 y^2 + \ldots \quad (9)$$

Extracting the 0^{th} order term in the temperature evolution (2) leads to:

$$\partial_t a = \frac{1}{\mathrm{Re}\,\mathrm{Pr}}\left(\partial_{xx} a + 2c + \partial_{zz} a\right) \quad (10)$$

At the wall, the molecular diffusion from the temperature variance budget is equal to $2\left\langle b'^2 + 2a'c' \right\rangle (\mathrm{Re}\,\mathrm{Pr})^{-1}$ (a' is the fluctuating part of a and <> denote average in time and in the homogeneous directions). Using (10), the asymptotic value of the molecular diffusion is:

$$MlDf \xrightarrow[y\to 0]{} \frac{2}{\mathrm{Re}\,\mathrm{Pr}}\left\langle b'^2 + \left(\partial_x a'\right)^2 + \left(\partial_z a'\right)^2 \right\rangle \quad (11)$$

At the wall, this term is the opposite of the dissipation rate. The first term is linked the fluctuating wall-normal temperature gradient (dominant for the isothermal configuration in the near-wall region). The second and third ones are connected with the fluctuating wall-parallel temperature gradient (dominant in the isoflux configuration in the near-wall region).

In figure 7, the molecular diffusion in the isothermal case is ≈ 7 times higher compared with the isoflux one: the Dirichlet boundary condition produces important fluctuations of the normal temperature gradient at the wall. Actually, the ratio of the molecular diffusion associated to the temperature variance budget between isoflux and isothermal configurations is equal to 0.13, which is lower than the values mentioned in Kasagi et al. (1989) and obtained with an unsteady 2D synthetic model; in the range [0.3-0.5].

The region around $y^+ \approx 5$ is also remarkable: isothermal and isoflux cases have almost the same molecular diffusion, slightly differing from the one obtained in the conjugate case. Results in the conjugate heat transfer configuration are not always in-between isothermal and isoflux ones. Moreover, they are closer to isothermal ones after $y^+ \approx 10$.

5 Turbulent Prandtl number

Geshev (1978), has derived analytically a turbulent Prandtl number (ratio of turbulent shear stress to heat flux) for isothermal and isoflux walls as well as conjugate cases. (eq. (13))

$$\left\langle u_2(y_1,t)u_2(y_2,t-\tau)\right\rangle \propto {y_1}^2 {y_2}^2 \exp\left(-\tau/\Delta\right) \quad (12)$$

$$\mathrm{Pr}_t = \mathrm{Pr}\,\frac{1 + \frac{{y^+}^2}{2\Delta} - \exp\left(-y^+/\sqrt{\Delta}\right)}{1 + \mathrm{Pr}\,\frac{{y^+}^2}{2\Delta} - \frac{\Lambda}{1+\Lambda}\exp\left(-y^+\sqrt{\mathrm{Pr}/\Delta}\right)} \quad (13)$$

Λ is the thermal activity ratio (which is also the thermal effusivity ratio) and Δ, defined via the spatio-temporal correlation of equation (12) is 20 according to Geshev (1978).

In figure 8, the agreement is qualitative ($\mathrm{Pr}_t \propto y^+$ at the wall for conjugate and isoflux configurations). This clearly shows that wall-modelling of temperature-related quantities inside the fluid should care for the thermal boundary condition when $y^+ \le 20$ and $\mathrm{Pr} \approx 1$. The Geshev model does not account for the wall-parallel diffusion and the source term. This may explain the overall underestimation of the turbulent Prandtl number.

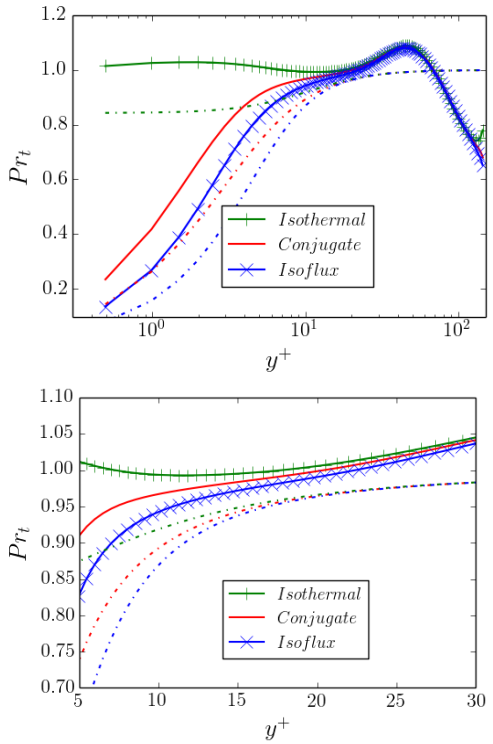

Figure 8: Turbulent Prandtl number. Lines: present. Dash-dotted lines: Geshev.

6 Velocity-temperature correlations

Abe et al. (2009) have investigated the normalized correlation between velocity and temperature: $corr = <UT> / U_{RMS} T_{RMS}$. In the isothermal case, the correlation between the streamwise velocity and the temperature reaches a peak for $y^+ \approx 7$.

In figure 9, almost the same peak is observed in the isothermal case. Our isoflux result is also in very good agreement with Tiselj et al. (2001a).

In figure 10, a trend similar to the one in figure 9 is observed: around $y^+ \approx 20$, the normalized correlation for conjugate heat transfer is close to the isothermal one while around $y^+ \approx 0$ it is almost equal to the isoflux one. This trend seems general as it is also observed in figure 7 for the molecular diffusion and dissipation rate of the temperature variance budget.

The loss of correlation between streamwise velocity and temperature at the wall is related to the presence of temperature fluctuations at the wall while the velocity components are constant.

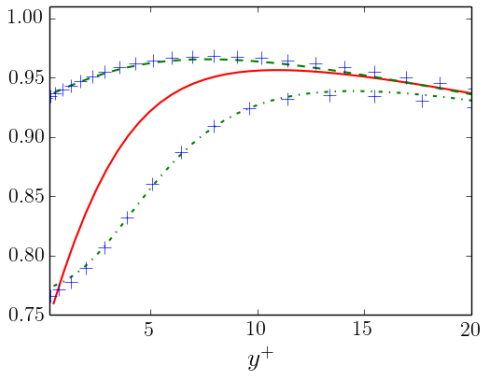

Figure 9: Correlation uT. Line: conjugate. Dashed line: isothermal. Dash-dotted line: isoflux. Symbols: Kasagi et al. (1992), Tiselj et al. (2001a).

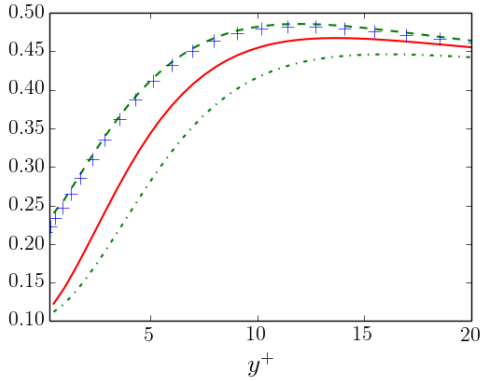

Figure 10: Correlation vT. Line: conjugate. Dashed line: isothermal b.c. Dash-dotted line: isoflux b.c. Symbols: Kasagi et al. (1992).

7 Fourier and Laplace analysis of the solid conduction

A solid domain, infinite in x and z directions and semi-infinite in the y direction is subjected to a thermal load at $y = 0$, which is statistically stationary and homogeneous in x and z. Applying a Fourier transform in time and in the homogeneous directions to the solid heat diffusion equation leads to:

$$ik_t \frac{\rho C_p}{\lambda} T_s = \partial^2_{yy} T_s - \left[k_x^2 + k_z^2\right] T_s \qquad (14)$$

The solid heat diffusion equation is linear: the general solution is a superposition of Fourier modes. k_t is the angular frequency while k_x and k_z are the wave-numbers in the streamwise and in the spanwise direction. When $k_t = 0$, the averaged temperature in the solid decreases exponentially:

$$T_s(y) \propto T_s(0) \exp\left(-|y|\sqrt{k_x^2 + k_z^2}\right) \qquad (15)$$

The characteristic penetration depth of temperature fluctuations δ satisfies:

$$\frac{1}{\delta^2} \propto k_x^2 + k_z^2 \qquad (16)$$

When $k_x = k_z = 0$, there is a phase shift between the temperature taken at different depths. However, the decay of the amplitude is still exponential and the characteristic penetration depth δ satisfies:

$$\frac{1}{\delta^2} \propto \frac{\rho C_p}{\lambda} k_t \qquad (17)$$

In the general case, the analysis is more complex. Applying a Laplace transform (denoted by an overbar hereafter) in y direction leads to:

$$\overline{\partial^2_{yy} T(y)} = s^2 \overline{T}(s) - s T_{y=0} - \partial_y T_{y=0} \qquad (18)$$

$$\overline{T} = \frac{s T_{y=0} + \partial_y T_{y=0}}{s^2 - \left(k_x^2 + k_z^2\right) - ik_t \dfrac{\rho C_p}{\lambda}} \qquad (19)$$

Applying partial fraction decomposition and an inverse Laplace transform leads to an exponential decay of the temperature fluctuations with a characteristic penetration depth satisfying equation 20:

$$\frac{1}{\delta^4} \propto \left(k_x^2 + k_z^2\right)^2 + \left(\frac{\rho C_p}{\lambda} k_t\right)^2 \qquad (20)$$

From this analysis, it is clear that large scale temperature fluctuations with a long lifespan are more likely to penetrate deep in the solid. It is often overlooked that structures highly localized in space and times are responsible for severe thermal constraint in the solid, near the fluid interface. A 1D model of solid heat diffusion that does not account for the lateral heat conduction ($k_x = k_z = 0$) may over-estimate δ and under-estimate the thermal constraint at the fluid interface.

The present analysis could be extended to domains with a finite length in the y direction. This involves Green functions. Such developments are more complex.

8 Analysis of temperature variance

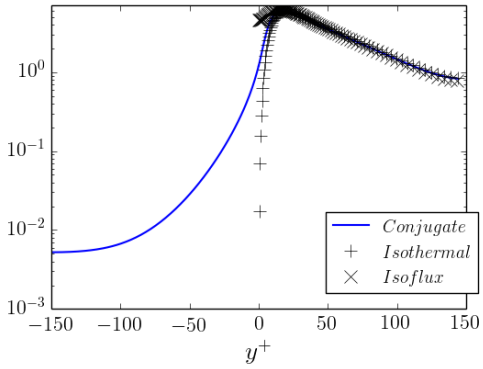

Figure 11: Temperature variance inside the fluid (y>0) and solid (y<0) domains.

Figure 11 shows that it is not possible to fit the temperature variance to an exponential curve (straight line in this linear-log plot) as it may be done for a given (k_x, k_z, k_t). As the turbulent forcing at the wall contains a broad range of spatial and temporal frequencies, the superposition of the exponentials may prevent a simple curve fitting to be efficient.

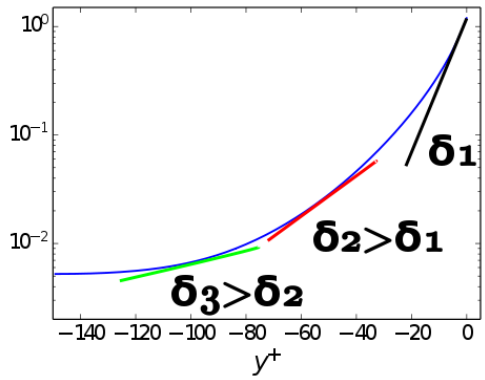

Figure 12: Temperature variance inside the solid domain.

At a given depth y_i, the slope of the temperature variance can be used to compute a characteristic length δ_i, as illustrated in figure 12. It is the low wave-number range of the fluctuating temperature spectrum that determine local $\delta_i(y^+)$ as the integral length-scale of the spectrum increases with increasing depth, as sketched figure 13. Considering the temperature variance is the squared temperature fluctuation and assuming $k_x = k_t = 0$, the length-scale in z associated with δ_1 is $\lambda_z^+ = 2\pi/k_z^+ = 79$. This is reasonably close to the spacing between velocity streaks ($\lambda_z^+ \approx 100$).

Indeed, from the theorem of Parseval, L2-norm is conserved during a Fourier transform. Therefore, at a given depth, the temperature variance scales with the integral of the squared spectrum (Fourier transforms in time and homogeneous directions). The decaying temperature variance in the solid domain should correspond to spectrum similar to the ones of figure 13.

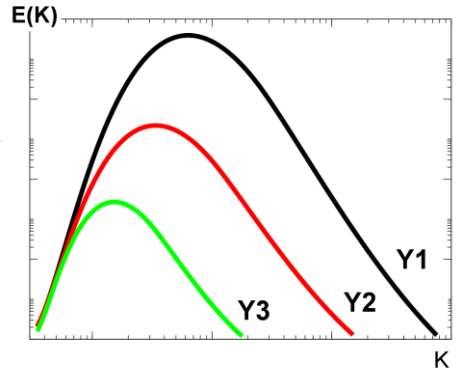

Figure 13: Conjectured spectrum of the fluctuating temperature in the solid domain at different depths.

However, our first simulation was not instrumented to extract the spectrum of temperature fluctuations inside the solid. This is an ongoing work. From the spectrum of the temperature and the heat flux at the wall, the temperature field inside a semi-infinite solid and any related statistical quantity can be theoretically reconstructed. It is delicate to extract such result because of the broad range of frequencies involved (high frequencies at the fluid interface and low frequencies at the outer wall).

Note that the imposed heat flux brings a null derivative of the temperature variance at the outer boundary. The solid heat diffusion equation being elliptic, the outer boundary condition impacts the whole thermal field. A boundary condition of Robin type may be more relevant since our solid domain is not semi-infinite.

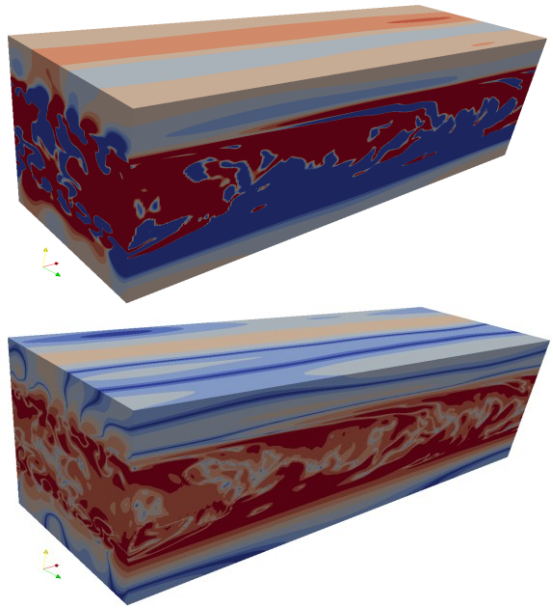

Figure 14: Instantaneous fluctuating temperature field in log scaling. Top: hot and cold spots. Bottom: absolute value.

9 Instantaneous temperature field

The instantaneous fluctuating temperature field in the domain is presented using a colour map in logarithmic scale because the fluctuations inside the solid have low amplitude compared to the ones in the fluid.

Some fluctuating spots have clearly penetrated the top wall. Very long thermal structures are also visible at the outer boundary of the wall. Their size suggests that the computational domain should be longer in x direction to capture faithfully the temperature fluctuations in the solid region.

10 Perspectives

The channel flow is one of the simplest geometries for a wall-bounded turbulent flow. It was selected to verify our developments. The ability to compute high-order statistics was established on an isothermal case. Then, the impact of the thermal boundary condition on the budgets of the heat fluxes and temperature variance was investigated.

From our results, it is clear that conjugate heat transfer provides different results compared with an imposed temperature or heat flux at the wall and that wall-parallel conduction together with topology of hot and cold temperature spots plays a significant role in the penetration depth of turbulent thermal loading. The authors are currently carrying out more simulations to extend the present analysis with larger domains than used for the classical channel flow DNS: the small wave-number range of the spectrum is of particular interest for conjugate heat transfer.

The objective behind the present DNS is to build a reference database focused on temperature-related statistics including conjugate heat transfer. The DNS results reported here are currently available on request and will be made publicly available on the user group of the Incompact3d website.

Acknowledgements

The authors thank Prof. I. Tiselj for providing results and assistance. We also thank the French National Research Agency and EDF R&D for funding the study and providing computational time on Zumbrota supercomputer (IBM – BlueGene/Q).

References

Abe, H., Antonia, R. A., and Kawamura, H. (2009). Correlation between small-scale velocity and scalar fluctuations in a turbulent channel flow. *Journal of Fluid Mechanics*, Vol. 627, pp. 1-32.

Chung, S. Y., and Sung, H. J. (2003). Direct numerical simulation of turbulent concentric annular pipe flow: Part 2: Heat transfer. *International journal of heat and fluid flow*, Vol. 24, pp. 399-411.

Geshev, P. I. (1978). Influence of heat conduction of the wall on the turbulent prandtl number in the viscous sublayer. *Journal of engineering physics*, Vol. 35, pp. 949-952.

Kang, S., Iaccarino, G., and Ham, F. (2009). DNS of buoyancy-dominated turbulent flows on a bluff body using the immersed boundary method. *Journal of Computational Physics*, Vol. 228, pp. 3189-3208.

Kasagi, N., Kuroda, A., and Hirata, M. (1989). Numerical investigation of near-wall turbulent heat transfer taking into account the unsteady heat conduction in the solid wall. *Journal of Heat Transfer*, Vol. 111, pp. 385-392.

Kasagi N., Tomita Y., and Kuroda A. (1992), Direct numerical simulation of passive scalar field in a turbulent channel flow, *Journal of Heat Transfer*, Vol. 114, pp. 598–606.

Laizet S. and Lamballais E. (2009), High-order compact schemes for incompressible flows: A simple and efficient method with quasi-spectral accuracy. *Journal of Computational Physics*, Vol. 228, pp. 5989–6015.

Laizet S. and Li N. (2011), Incompact3d: A powerful tool to tackle turbulence problems with up to $o(10^5)$ computational cores. *International Journal for Numerical Methods in Fluids*, Vol. 67, pp. 1735–1757.

Lamballais, E., Fortuné, V., and Laizet, S. (2011). Straightforward high-order numerical dissipation via the viscous term for direct and large eddy simulation. *Journal of Computational Physics*, Vol. 230, pp. 3270-3275.

Orszag S. A. (1971), Numerical simulation of incompressible flows within simple boundaries: I-galerkin (spectral) representations, *Journal of Fluid Mechanics,* Vol. 49, pp. 75–112.

Tiselj I., Bergant R., Mavko B. et al. (2001a), DNS of turbulent heat transfer in channel flow with heat conduction in the solid wall, *Journal of heat transfer*, Vol. 123, pp. 849-857.

Tiselj, I., Pogrebnyak, E., Li, C., Mosyak, A., and Hetsroni, G. (2001b). Effect of wall boundary condition on scalar transfer in a fully developed turbulent flume. *Physics of Fluids*, Vol. 13, pp. 1028-1039.